Title

Tunable Permeability of Cross-Linked Microcapsules from pH-Responsive Amphiphilic Diblock Copolymers: A Dissipative Particle Dynamics Study

Journal

Langmuir, 33(29)

ISSN

0743-7463

Authors

Wang, Zhikun
Gao, Jianbang
Ustach, Vincent
et al.

Publication Date

2017-07-25

DOI

10.1021/acs.langmuir.7b01586

Peer reviewed

Tunable Permeability of Crosslinked Microcapsules from pH-Responsive Amphiphilic Diblock Copolymers: A Dissipative Particle Dynamics Study

Zhikun Wang[1,2], Jianbang Gao[1], Vincent Ustach[2], Chunling Li[1,3], Shuangqing Sun[1,3], Songqing Hu[1,3,*], Roland Faller[2,*]

[1]*College of Science, China University of Petroleum (East China), 266580 Qingdao, Shandong, China*

[2]*Department of Chemical Engineering, UC Davis, 95616 Davis, California, USA*

[3]*Key Laboratory of New Energy Physics & Materials Science in Universities of Shandong, China University of Petroleum (East China), 266580 Qingdao, Shandong, China*

ABSTRACT:

Using dissipative particle dynamics simulation, we probe the tunable permeability of crosslinked microcapsules made from pH-sensitive diblock copolymers poly(ethylene oxide)-b-poly(N,N-diethylamino-2-ethylmethacrylate) (PEO-b-PDEAEMA). We first examine the self-assembly of non-crosslinked microcapsules and their pH-responsive collapse, then explore the effects of crosslinking and block interaction on swelling or deswelling of crosslinked microcapsules. Our results reveal a preferential loading of hydrophobic dicyclopentadiene (DCPD) molecules in PEO-b-PDEAEMA copolymers. On reduction of pH, non-crosslinked microcapsules fully decompose into small worm-like clusters due to large self-repulsions of protonated copolymers. With increasing degree of crosslinking, the morphology of the microcapsule becomes more stable to

pH change. The highly crosslinked microcapsule shell undergoes significant local polymer rearrangement in acidic solution, which eliminates the amphiphilicility and therefore enlarges the permeability of the shell. The responsive crosslinked shell experiences a “disperse-to-buckle” configurational transition on reduction of pH, which is effective for steady or pulsatile regulation of shell permeability. The swelling rate of the crosslinked shell is dependent on both electrostatic and non-electrostatic interactions between the pH-sensitive groups as well as the other groups. Our study highlights the combination of crosslinking structure and block interactions in stabilizing microcapsules and tuning their selective permeability.

1. INTRODUCTION

Microcapsules from amphiphilic block copolymers that are sensitive to external stimuli have great potential for applications in nanotechnology, optoelectronics and nanomedicine[1-4]. Triggered by environmental stimuli such as temperature, pH, light, salt and magnetic fields, block copolymers can undergo conformation transitions which can in turn induce swelling or collapse of microcapsule shells and eventually lead to exchange of particles in or out of the microcapsule[5-7]. There is considerable interest in using stimuli-responsive microcapsules as carriers of special solutes for long-term preservation and stimulus controlled release, e.g., loading/release of encapsulated drugs or curing agents on changes of pH in tumor tissues or corroded steels, respectively[3,8]. The high sensitivity of microcapsules can be attributed to a structural transition (swelling or degradation) of shell copolymers caused by variations of charge, redox potential, mobility, etc. of functional groups in response to

stimulus changes[1,9]. Other factors including chain architecture, solvent, concentration, ionic strength, etc., can affect the self-assembly of block copolymers and contribute to the stability and sensitivity of responsive microcapsules[10,11]. Architecture and chemistry of block copolymers have been successfully exploited to create responsive microcapsules that release encapsulated solutes on demand[5,9].

Microcapsules self-assembled from block copolymers are stabilized by the interface-driven force above the critical micelle concentration, and their stability can be affected by many external conditions (e.g., stimuli, dilution, and agitation)[12]. To improve the stability of the nanostructure, covalent crosslinking between block copolymers has been developed as an effective method for creating nano-objects with very long retention times[4,13]. A number of block copolymer multicompartment micelles with crosslinked core or shell domains have been tested for enhancing their dynamical and structural stabilities in response to stimulation[10,14-19]. In addition to enhancing stability, the linker molecules can add functionality, and cargo loading could be improved[10,14-19]. Crosslinking can also lead to a loss of permeability, fluidity, and bendability of the microcapsule shell due to increased mechanical stress and fluid induced viscous stress[20]. Therefore, crosslinking likely changes the stimulus response of microcapsules. Great efforts have been made to improve the sensitivity of highly crosslinked microcapsules while maintaining stability[21-23]. An effective and efficient approach is to incorporate functional groups that are sensitive to a particular type of external stimulus to block copolymers as the initiator of micellar structural or dynamical responses. The high flexibility in the chemical design of block polymers

and linkers allows the formation of crosslinked microcapsules with versatile structures and chemistries, which lead to tunable responsive behavior of microcapsules on changes of external stimuli through reversible structural transitions and self-adjustment of physicochemical properties[21-23].

Despite recent progress in synthesis and characterization of crosslinked block copolymer nanoparticles, the development of multifunctional carriers with tunable responsive permeability remains a challenge. Due to the great complexity of the network-like structure, it is difficult not only to rationally design experiments but also to develop theoretical models predicting the dynamics of these systems[24]. The diffusion of particles in or out of crosslinked microcapsules involves multiple time and length scales, and is dependent on tight coupling of elastic and viscous stresses, which makes the stimuli responsive mechanisms of crosslinked nanostructures more complex than non-crosslinked nanoassemblies[16,25,26].

Molecular dynamics (MD) is effective in revealing the underlying mechanism of stimuli responsive polymer systems[27-29]. It can deal with responsive behaviors of polymer systems over short time and length scales often better than experiments. Dissipative particle dynamics (DPD) has been successfully used to create pH-sensitive block copolymer microcapsules that can load or release solutes on demand[30-33]. There is, however, little computational work exploring crosslinked block copolymers due to the difficulty in building suitable models. MD for crosslinked polymeric systems focusses on microgel systems or crosslinking epoxy resin materials[24,34-41]. A recent DPD study suggests that the responsive swelling and de-

swelling of the network-like gel can effectively induce steady and pulsatile release of encapsulated solutes[24].

Here, we introduce a mesoscale model of crosslinked pH-sensitive block copolymer microcapsules using DPD. Based on nearest neighbor bonding[34-38], we developed an efficient cyclic method for crosslinking block copolymers that allows to directly probe the effect of crosslinking on the tunable permeability of the microcapsules. We model the diblock copolymer poly(ethylene oxide)-b-poly(N,N-diethylamino-2-ethylmethacrylate) (PEO-PDEAEMA) as the shell, and dicyclopentadiene (DCPD) as the core of our microcapsule model. PDEAEMA is a cationic polymer which has attracted considerable attention for pH-responsive polymer materials, both as homopolymer and as block copolymers, such as PEO-PDEAEMA[42-46]. PDEAEMA segments are hydrophobic (in basic solution) and drive the formation of micelles, which can be stabilized by hydrophilic PEO segments. The cationic PDEAEMA segments are also able to bind to negatively charged groups to form complexes[42,43]. In this work, the appearance and structure of microcapsules were studied in both the normal state (basic conditions) and the swollen state (acidic conditions), and of pH-induced changes are discussed.

2. METHODOLOGY

2.1. Dissipative Particle Dynamics

Dissipative particle dynamics (DPD) simulation combines a soft repulsive potential and a momentum-conserving thermostat to control the interactions of beads representing clusters of atoms, e.g., repeat units in a polymer. The force acting on

bead *i* can be described as[47]

$$f_i = \sum_{i \neq j} (F_{ij}^C + F_{ij}^D + F_{ij}^R) \quad (1)$$

where F_{ij}^C is the conservative repulsive force modeling excluded volume, F_{ij}^D is the dissipative force modeling viscous drag which depends on the relative positions and velocities of moving beads, F_{ij}^R is a random force acting on a bead pair. The sum runs over all beads *j* within a cutoff radius r_c around bead *i*. F_{ij}^D and F_{ij}^R act together as a momentum conserving thermostat. A simple harmonic spring force $f_i^S = \Sigma_j C\mathbf{r}_{ij}$ is added to the total force f_i to describe bond stretching interactions, where *C* is the spring constant. The excluded volume F_{ij}^C is described by

$$F_{ij}^C = \begin{cases} a_{ij}(1 - r_{ij}/r_{cut}) & (r_{ij} < r_{cut}) \\ 0 & (r_{ij} > r_{cut}) \end{cases} \quad (2)$$

where the constant a_{ij} describes the repulsive interaction between beads *i* and *j*, and $\mathbf{r}_{ij} = \mathbf{r}_i - \mathbf{r}_j$. If we use $a_{ii} = a_{jj}$, the repulsive parameters a_{ij} can be obtained from Flory-Huggins parameters χ_{ij}[48]

$$a_{ij} = a_{ii} + 3.50c_{ij} \quad (3)$$

$$c_{ij} = \frac{\Delta E^{mix} V_r}{RT\phi_i \phi_j V} \quad (4)$$

while χ_{ij} is mapped from a long chain to a short DPD chain and bridges the gap between atomistic MD and mesoscale DPD methods. *R* is the gas constant and *T* temperature, ϕ_i and ϕ_j are volume fractions of beads *i* and *j*, respectively, *V* is the total

volume and V_r is a reference volume. ΔE^{mix} is the mixing energy of two different types of beads which can be estimated by

$$\Delta E^{mix} = E_{ij} - (E_i + E_j) \quad (5)$$

where E_{ij}, E_i and E_j are the total potential energy of a binary mixture, and the potential energies of pure components i and j, respectively. ΔE^{mix} has been determined by MD simulations using the COMPASS force field in which the potential energy is expressed as $E = E_{bonded} + E_{nonbonded} + E_{cross}$. E_{bonded} includes bond stretching, bond bending, dihedral torsion and out-of-plane bending. E_{cross} indicates cross terms between different bonded terms. $E_{nonbonded}$ includes van der Waals and electrostatic interactions.

2.2. Coarse-Grained Models and Input Parameters

The coarse-grained molecular model of PEO-b-PDEAEMA is shown in Figure 1. The block lengths ensure that hydrophobic cargo can be well encapsulated by this polymer and a well crosslinked microcapsule shell structure can be obtained. The polymer was divided into three types of beads. Two EO repeat units are merged into one DPD bead, whereas one repeat unit of DEAEMA was split into two beads (MMA and DEA). In acidic solution we have the protonated version DEAH, which is assumed to have the same size as DEA. The protonation degree of the pH-sensitive groups can be calculated by the Henderson-Hasselbalch equation from the pK_a and pH values of the solution:[49]

$$P_d^+ = (1 + 10^{\mathrm{pH} - \mathrm{p}K_a})^{-1} \times 100\% \quad (6)$$

where P_d^+ is the protonation degree; the pK_a is 6.9 for the PDEAEMA block[33]. If we assume that a P_d^+ < 3% can be modelled as fully deprotonated and a P_d^+ > 97% can be assumed as fully protonated we get a pH of 8.4 or above for the fully deprotonated (basic) case and a pH of 5.4 or below for the fully protonated (acidic) case.

A DCPD molecule was represented by two bonded DPD beads, and five water molecules were merged into one DPD bead (W). All beads have the same volume and mass of 150 Å^3 and 90 amu[48].

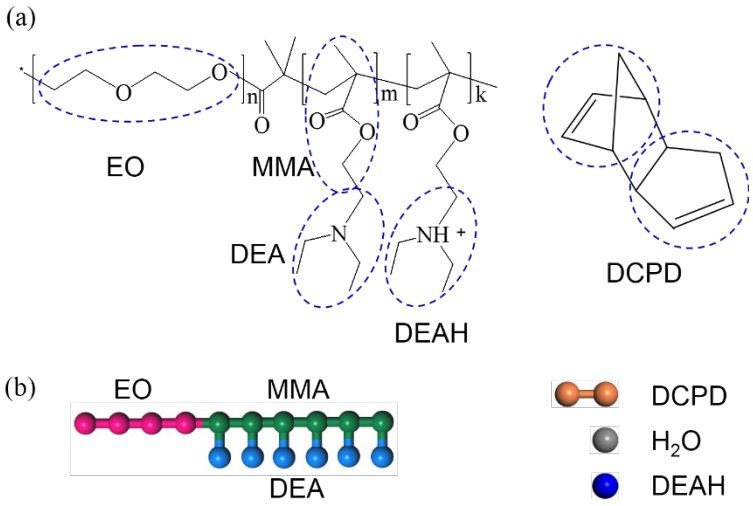

Figure 1. Atomistic structures and coarse-grained representations of PEO-b-PDEAEMA, DCPD and H_2O.

To calculate the conservative force constants, EO, MMA and DEA monomers were end-capped by methyl groups. In acidic solution, DEA is protonated at its tertiary amine groups to obtain DEAH, and Cl^- ions were added for electrical neutrality. Pure and binary systems were built by the Amorphous Cell algorithm in Materials Studio (Accelrys Inc.) and subsequently subjected to up to 10,000 steps of

energy minimization until an energy convergence of 0.0001 kcal/mol and a force convergence of 0.005 kcal/mol/Å were reached. The cutoff distance for van der Waals interactions was 12.5 Å, with a spline width of 1 Å and a buffer width of 0.5 Å. Ewald summation was used with an accuracy of 0.001 kcal/mol. Both, pure and binary systems we simulated for 2 ns under NPT condition, at 298 K and 1 atm controlled by the Nosé-Hoover[50] (Q ratio is 0.01, decay constant is 0.1 ps) and Berendsen[51] (decay constant is 0.1 ps) methods, respectively, and the final 1 ns was used to calculate the potential energy.

Table 1. Conservative force constants a_{ij} used by DPD simulations

	EO	MMA	DEA	DEAH	DCPD	W
EO	25					
MMA	37.04	25				
DEA	41.40	30.44	25			
DEAH	30.30	146.06	--	50		
DCPD	62.79	59.60	25.21	150.18	25	
W	26.05	76.18	127.65	26.40	88.49	25

All DPD simulations were conducted using the Mesocite DPD module in Materials Studio. The conservative force constants for DPD simulations are listed in Table 1. The positive charges on the protonated DEAH beads in acidic solution were implicitly taken into account by increasing the repulsion between DEAH beads to 50. The cutoff r_{cut}, bead mass m and thermal energy k_BT (= 1) serve as units for length, mass and energy, respectively. Based on the bead volume, r_{cut} was set to $\sqrt[3]{3 \cdot V_{bead}}$ = 7.66 Å at ρ = 3. The DPD time scale was $t = r_{cut}\sqrt{m / k_BT}$ = 0.0046 ns at 298 K. The dissipative strength is 4.5. The harmonic spring constant was set to 4.0, and no angles or dihedrals were included. The simulation box size was

250×250×250 $Å^3$ (32.6×32.6×32.6 r_{cut}^3) containing $1.046×10^5$ beads. The time step was 0.05, and the equilibrium simulations for self-assembly in basic conditions (defined as 0% protonated, pH > 8.4) and after pH-response in acidic conditions (defined as 100% protonated, pH < 5.4) lasted both $5×10^5$ steps (115 ns) unless otherwise stated.

2.3. Construction of Crosslinked Microcapsule

A widely used nearest neighbor bonding principle[34-38] was used to build the crosslinked microcapsule from a self-assembled microcapsule with PEO-b-PDEAEMA shell and DCPD core. DEA beads on copolymers were possible crosslinking points, and an extra hydrophobic linker molecule was used to connect DEA beads on copolymers. The linker molecule contains only one bead (to minimize the effect of additional beads on model density), and has the same repulsive parameters as MMA with other beads (to maintain the hydrophobicity of the crosslinked PDEAEMA blocks). Specifically, three cyclic dynamic processes were used to build the crosslinked microcapsule:

- Distances between all DEA pairs were monitored and the closest pairs detected;
- If a distance was smaller than a threshold, r_{th}, a linker bead was created at the center of the two DEA beads, and covalently bond them together;
- A geometry optimization using the conjugate gradient algorithm and a DPD simulation of 1000 steps remove internal stresses and geometric distortions;
- A larger distance (r_{th} + 1 Å) was used as the new threshold to increase the crosslinking degree (i.e., the number of existing linker-DEA bonds divided by the

total number of DEA beads), and the above three steps were repeated. Note that only one linker-DAE bond could be formed for a single DAE bead. The process stops if a desired crosslink degree was obtained.

The threshold r_{th} was ranging from 5 to 15 Å, which leads to crosslinking degrees from 0 to 90%. To avoid self-crosslinking only pairs on different molecules were considered. The box size was fixed during crosslinking as the additional linker beads lead to only a small variation of the overall density (<5% for all models in this work) and has little influence on the considered properties. The above process was implemented using the Scripting Interface in Materials Studio. It was chosen to be a computationally effective way to mimic the fundamentals of crosslinking. Figure 2 gives a schematic illustration of the crosslinking structure in the block copolymer shell.

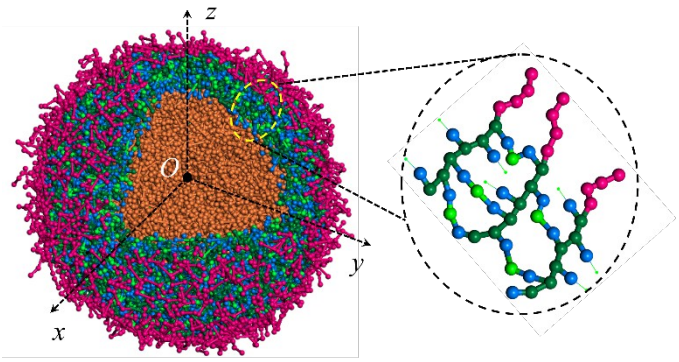

Figure 2. Schematic illustration of a crosslinked microcapsule. Color scheme: EO-pink, MMA-dark green, DEA-blue, linker-light green, DCPD-orange. Some crosslinking points in the enlarged region are shown with green dots for illustration.

2.4. Calculation of Contact Probability

We use contact statistics from the DPD simulations to reveal swelling or de-

swelling of the polymer shell based on changes of pH. Voronoi tessellation has been used to determine molecular contacts in the models [52]. Figure 3 shows the tessellation of a two-dimensional space applied to a set of beads, in which the black lines indicate the bounds (i.e., contact surfaces) of neighboring cells. The model is divided into polyhedral cells which contain the space closest to a given bead. The areas of contact surfaces between different cells are used to determine contact statistics of beads in DPD simulations. The contact statistics of beads in the present work is calculated by the voro++ 0.4.6 software[53]. The contact probability (*CP*) describes the contact statistics of two specific types of beads. For example, $CP_{A\text{-}B}$ indicates the proportion of the contact surface area between neighboring A and B beads, $S_{A\text{-}B}$, to the total surface area of A beads, S_A, i.e., $CP_{A\text{-}B} = S_{A\text{-}B} / S_A$. $CP_{A\text{-}B}$ ranges from 0 to 1, where 0 indicates no contact between A and B and 1 indicates A particles are completely surrounded by B particles.

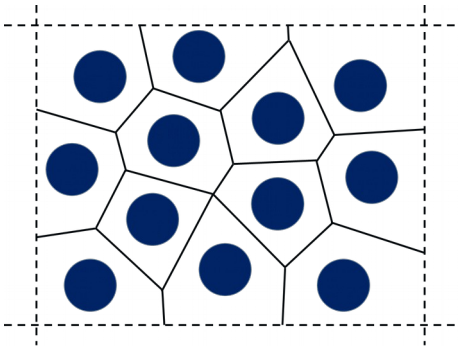

Figure 3. Voronoi tessellations applied to a set of beads in two-dimensional space.

3. RESULTS AND DISCUSSION

3.1. Formation and pH-Responsive Collapse of PEO-b-PDEAEMA Microcapsules

Cooperative self-assembly of the PEO-b-PDEAEMA / DCPD mixture in aqueous solution was explored as a function of the relative volume fraction of polymer and cargo, ϕ_P and ϕ_D, respectively (Figure 4). The self-assembly of pure polymers is shown in Figure S1 in Supporting Information as a reference. Within the considered range of volume fraction, capsule-like micelles with separated DCPD and PEO-b-PDEAEMA domains were obtained, in which DCPD molecules form an aggregated micelle, and PEO-b-PDEAEMA copolymers locate at the DCPD/water interface. The shell coverage and thickness of the equilibrium capsule depend on the ratio of $\phi_P : \phi_D$. For example, a decreasing trend of shell coverage was observed with fixed ϕ_P and increasing ϕ_D, while an increasing trend of shell thickness was observed with fixed ϕ_D and increasing ϕ_P. Also, a shape transition of the entire capsule from sphere, cylinder to incomplete lamella was observed at large values of ϕ_P or ϕ_D.

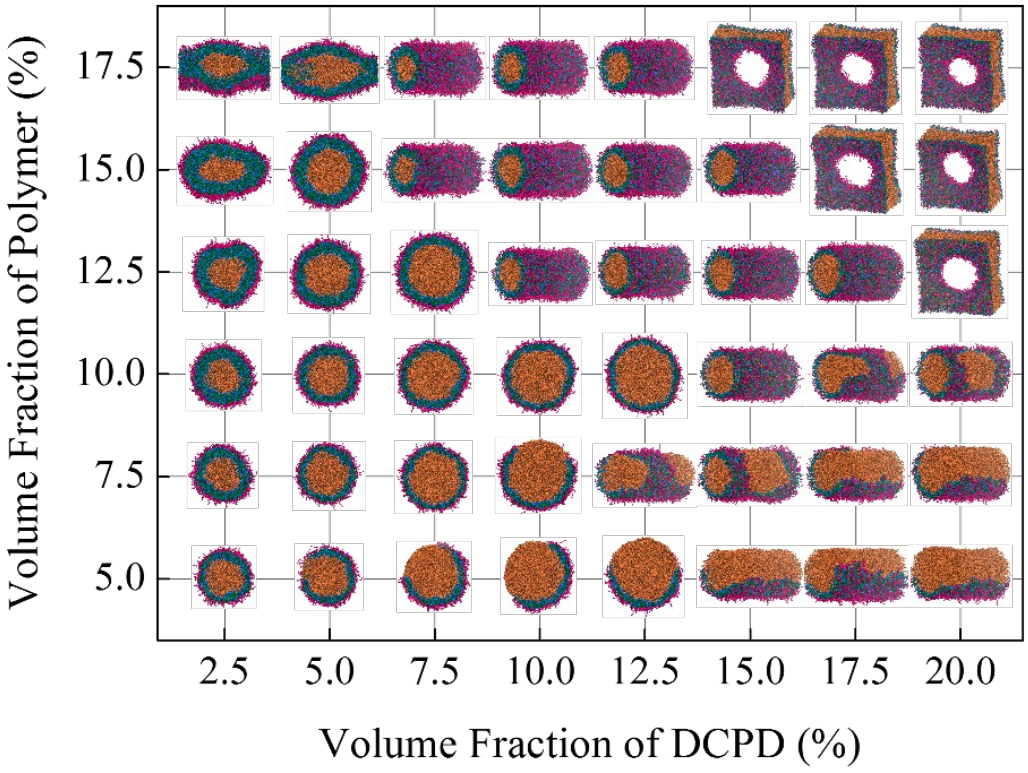

Figure 4. Morphologies of the system versus relative volume fraction of PEO-b-PDEAEMA (ϕ_P) and DCPD (ϕ_D). Spherical micelles are shown in cross sections. Color scheme as in Figure 1.

From a thermodynamic point of view, the co-assembly of the mixture is determined by three competing contributions: free energies of the core, interface and shell, to reduce the total free energy of the system[12,31]. The preferential location of the aggregated DCPD at the core is due to the high hydrophobicity of DCPD ($a_{DCPD\text{-}W}$ = 88.49) leading to lower dissolution energy, while the preferential encapsulation trend of PEO-b-PDEAEMA at the DCPD/water interface is due to the high compatibility of DCPD and DEA beads ($a_{DCPD\text{-}DEA}$ = 25.21) leading to lower interfacial energy. Since the hydrophobic repulsion between the core and water is proportional to the exposed area of DCPD, the interfacial tension (i.e., interface energy) is decreased by increasing shell coverage. The shell is spherical in order to reduce segmental interactions and increase configurational entropy[12]. With complete shell coverage, a slight increase of polymer concentration will lead to larger block stretching and the self-repulsive interaction of the copolymers will be increased, which leads to increased shell thickness[12].

Dynamic co-assembly of the encapsulation shells was also investigated for two representative models with complete spherical (ϕ_P : ϕ_D = 12.5% : 7.5%) and cylindrical (ϕ_P : ϕ_D = 12.5% : 12.5%) shells (Figure 5). Here, DCPD loading in PEO-b-PDEAEMA shell follows the adsorption-growth-micellization mechanism. The two components are initially homogeneously mixed. PEO-b-PDEAEMA and DCPD both assemble into small clusters and adsorb onto each other (0.12 ns). When the clusters

grow, capsule-like micelles with DCPD encapsulated by PEO-b-PDEAEMA are obtained, reducing surface tension (0.46 ns). Then, these microcapsules integrate further (0.92 ns) and finally form one big micelle with all DCPD enclosed by PEO-b-PDEAEMA (11.51 ns). The formations of spherical and cylindrical micelles follow the same mechanism. The equilibrium microcapsules have the largest loading efficiency for DCPD molecules. The loading efficiency is dependent on both the hydrophobicity of core molecules and the attraction between core molecules and hydrophobic blocks[54,55]. The force field in the present work includes interactions favorable for micellization and encapsulation of core molecules. The large loading efficiency enables better examination for the pH-responsive transition of the block copolymer shell.

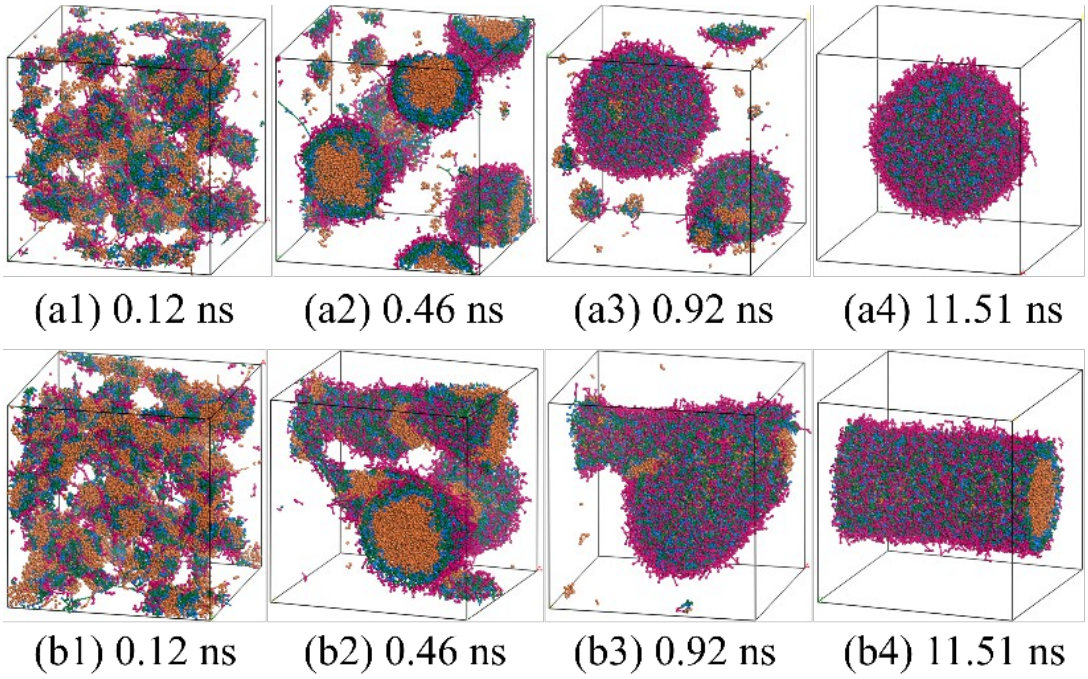

Figure 5. Encapsulation processes of DCPD in PEO-PDEAEMA with relative volume fractions of ϕ_P : ϕ_D = 12.5% : 7.5% (a1 ~ a4) and 12.5% : 12.5% (b1 ~ b4), respectively (basic solution, no

protonation). Color scheme as in Figure 1.

As experimentally observed, block copolymer micelles have a structural transition upon reducing pH (protonation) due to swelling of protonated PDEAEMA, which increases permeability[56,57]. The pH-responsive structural transition of PEO-b-PDEAEMA shell and encapsulation variation of the DCPD core were studied. Figure 6 shows the dynamic response of representative spherical and cylindrical microcapsules to pH reduction (full protonation). At first, the copolymer shell stays compact and closed (0 ns). Upon protonation of DEAH, the shell becomes looser and porous (1.15 ns), and gradually decomposes into multiple small worm-like clusters which move away from the shell into the water (4.62 ns). Finally, the copolymer clusters are totally dispersed in water and the DCPD micelle is almost completely exposed to water (57.71 ns). During the transition, the core DCPD remains stable due to the DCPD/water interfacial energy[32,58]. The decomposition of the PEO-b-PDEAEMA shell is mainly attributed to the combined contribution of electrostatic (DEAH-DEAH pairs) and non-electrostatic (DEAH-W, DEAH-MMA and DEAH-DCPD pairs) repulsions. Due to the interaction parameters in acidic solution (Table 1), the large repulsive forces between DEAH-DEAH and DEAH-MMA pairs lead to swelling of the PDEAEMA layer, the large attractive force between DEAH-W pairs increases hydrophilicity (i.e., solubility) of PDEAEMA, and the repulsive force between DEAH and DCPD leads to the detachment of polymers from the DCPD surface. As a result, the block copolymers form small clusters with DEAH and EO beads occupying the micelle/water interface and MMA beads inside. The structure

and dynamic of the non-crosslinked shell exhibit high sensitivity to a drastic pH change.

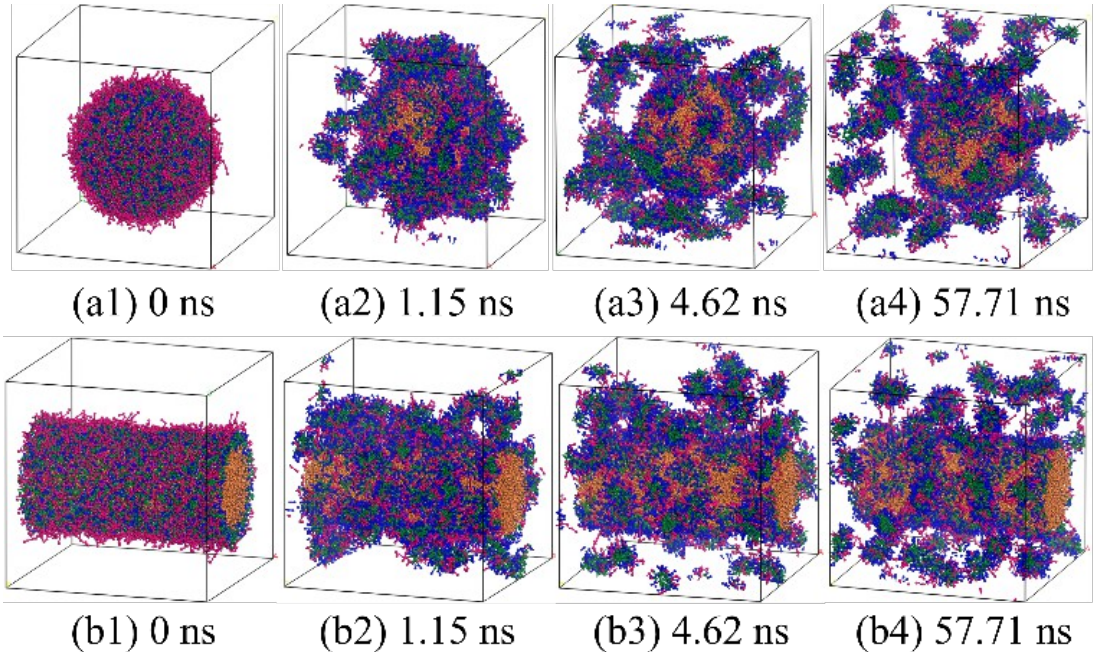

Figure 6. pH induced structural transformations of the spherical (a1 ~ a4) and cylindrical (b1 ~ b4) microcapsules due to switch from basic (no protonation) to acidic (full protonation) solution. Color scheme as in Figure 1.

3.2. Effect of Crosslinking on Swelling of Microcapsules

For nanoassemblies of individual block copolymers, the response can be tuned by covalently crosslinking different blocks[56]. In the present microcapsule, crosslinking of adjacent PDEAEMA blocks has been used to tune the pH-induced transition of the polymer shell. The effect of crosslinking on the radial density distribution of polymer beads is shown in Figure 7a (basic conditions). With increasing crosslinking degree, the shell density (peak height) is slightly increased and the thickness (peak range) slightly reduced. This is different than in other studies where increasing the crosslinking degree has led to a larger density and shrinkage of polymer materials[35,36]

Here, the addition of hydrophobic linker molecules during crosslinking increases the pressure and leads to swelling of the shell. The full width at half maximum *h* defines the thicknesses of the shells at around 26 ~ 27 Å for our range of crosslinking.

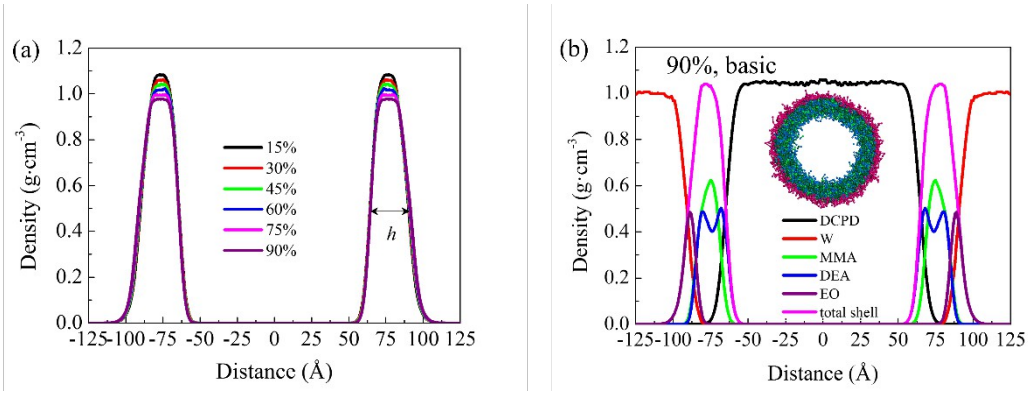

Figure 7. Density profiles of the polymer shell for different crosslinking degrees (a), and detailed distributions of shell, water and core beads in the 90% crosslinked model (b), as a function of distance from the center of mass of the microcapsule (ϕ_P : ϕ_D = 12.5% : 7.5%) in basic solution. Inset: cross section of the polymer shell.

Figure 7b presents the radial density profiles of all bead types in the 90% crosslinked microcapsule. Water and DCPD stay exclusively outside and inside of the microcapsule, respectively. Hydrophilic EO beads are located mostly at the shell/water interface, while hydrophobic MMA beads exhibit a large tendency to occupy the center of the shell. DEA beads occupy both the shell center and the shell/core interface. Overall, the shell has a distinct hydrophilic-hydrophobic separation of polymer beads isolating water molecules from core molecules. The crosslinking increases the mechanical stresses in the elastic network and leads to stronger viscous stresses for particle permeation (i.e., lower permeability)[24].

Upon pH reduction (protonation) the microcapsule shell undergoes a structure

transition due to the variation of interactions between protonated DEAH beads and other beads. Figure 8 presents the equilibrium morphology of polymers in highly acidic solution as a function of crosslinking degree. At low crosslinking (≤ 30%), the shell decomposes into small spherical or worm-like clusters with DEAH and EO beads exposed to water and MMA beads inside. At intermediate crosslinking (about 45%), the protonated polymers maintain the spherical morphology in general, but exhibit a number of large defects (holes or loosely attached clusters) in the shell. Further increase of crosslinking (≥ 60%) raises the compactness of the crosslinked shell gradually, and the overall morphology of the microcapsule is unchanged. The dynamics of the radius of gyration of the shell as a function of time (Figure S2 in Supporting Information) indicates that the size of the shell is rapidly increasing with pH reduction and fluctuates with time. Larger crosslinking degrees lead to smaller equilibrium radius of gyration, i.e., more closely packed shell. As expected, the crosslinking of PDEAEMA blocks plays a profound effect in hindering the collapse of shell copolymers, except for significant local rearrangements of polymer beads. The network structure in highly crosslinked shells has a large rigidity and is able to withstand the pressure exerted by the protonated shell.

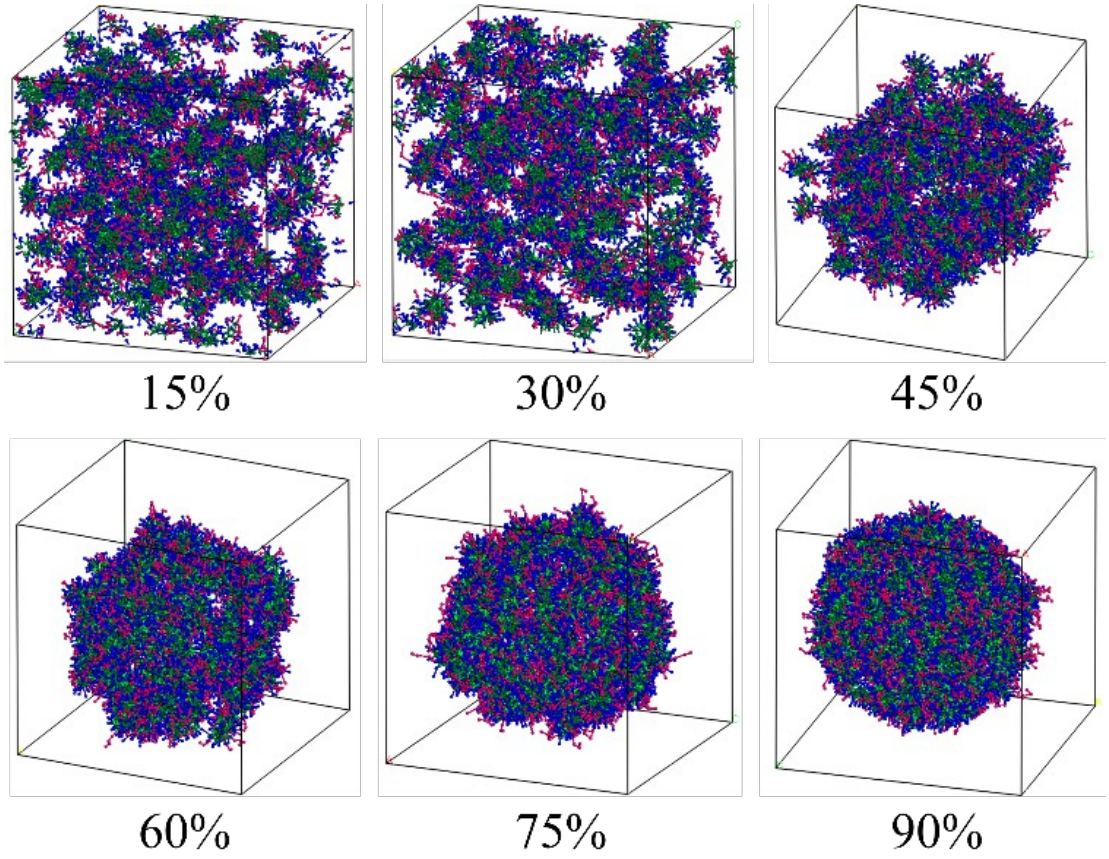

Figure 8. Morphological variation of the polymeric shells as a function of crosslink degree in acidic solutions. Water and DCPD beads are hidden for clarify. Color scheme as in Figure 1.

The effect of crosslinking degree on the stability of the shell was quantitatively studied by mean square displacements (*MSD*) of whole polymers in both basic and acidic solutions (Figure 9a). Variations of *MSD* curves at the two pH conditions show similar trend versus crosslinking. With increasing crosslinking, the *MSD* is decreased ≤ 60% but increased again above ≥ 75% crosslinking. The initial reduction of the *MSD* indicates that the dynamic stability of the block copolymer shell has been enhanced by crosslinking, especially for micelles in the acidic solution in which the *MSD* of the 15% model is approximately two orders of magnitude larger than that of the 60% model. The increasing crosslinking degree (crosslinking nodes) will further

restrict the segmental movement of polymers and lead to reduction of the shell mobility. We also clearly see subdiffusive regimes at short to intermediate times which are indicative of internal chain modes. However, the formation of the network structure does not always leads to the decrease in shell self-diffusion. The *MSD* at ≥ 75% exhibits a slight rising trend with increasing crosslink degree, especially for low pH. We attribute this behavior to the additional hydrophobic linker beads in the crosslinked shell, which lead to larger self-repulsion between polymer beads and increase the instability of the shell. Further, both, the chemical and architectural properties of linker molecules play an important role in the dynamic stability of the crosslinked structure[14-19]. The increase of the linker length or the incompatibility between linker and other beads will increase self-diffusion.

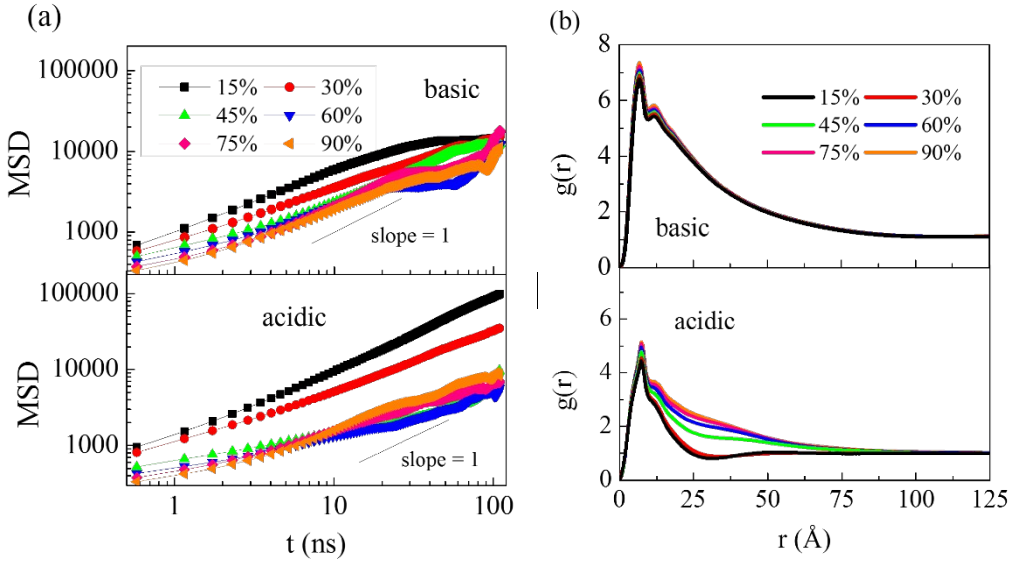

Figure 9. Mean square displacements (a) and radial distribution functions (b) of the polymer shell with different crosslinking degrees in basic and acidic solutions.

The effect of crosslinking on the packing of shell was studied by plotting the

radial distribution functions (*RDF*) of polymers in both basic and acidic solutions (Figure 9b). *RDF* curves at both conditions show peak positions at approximately 7.5 Å and 13.0 Å for all crosslinking values, corresponding to the average distances between first and second neighbors of bonded beads. With increasing crosslinking, the peak height is slightly increased indicating a shrinkage trend of the polymer shell, i.e., decrease of porosity. A long-range drop is observed after the two peaks due to the joint connection of polymer beads in the crosslinked shell, except below 30% crosslinking in acidic conditions since polymers are decomposed into small clusters. In particular, the *RDF* curves show no discrepancy at high crosslinking indicating that the shell is unchanged. In this condition, the internal pressure of the shell will be increased due to the additional hydrophobic linkers, leading to larger self-diffusion of the shell. This explains the above mentioned increase of *MSD* at ≥ 75%. From Figure 9a and 9b, the self-diffusion (dynamical) and packing (structural) properties for highly crosslinked shells are competing in response to the variation of crosslink degree. Our simulations highlight the conflicting effect of crosslinking features (including variations in crosslink density, linker chemistry and architecture, etc.) on the thermodynamic stability of the microcapsule.

The configuration of the crosslinked polymer shell at reduced pH undergoes a significant change, as indicated by the radial density profiles of all bead types in the 90% crosslinked system (Figure 10a). The hydrophilic EO beads and the hydrophobic MMA beads both locate across the full range, while protonated DEAH beads exhibit two peaks near the outer shell/water and shell/DCPD interfaces. Water molecules

enter the polymer shell. DCPD beads stay inside the microcapsule due to its large hydrophobicity. The cross section of the protonated shell (inset) shows an amorphous rearrangement of polymer beads at acidic conditions, in comparison with that in Figure 7b (basic). This configuration change leads to the disappearance of amphiphilicity and the shell becomes permeable for water. Moreover, from the radial density distribution ranges of the shell in Figure 7b and Figure 10a, the shell thickness has been expanded in response to pH reduction, which leads to a highly porous internal structure[24,30]. Figure 10b shows a divided morphological distributions of MMA, linker and DEAH beads in a local region of the 90% crosslinked shell. MMA beads, which are backbone of block PDEAEMA, form buckled worm-like clusters; the linker beads co-locate with MMA; DEAH beads are widely distributed regardless of the other beads. The cavities in the buckling structure are due to the relative weak crosslinking (e.g., local crosslink degree) in these domains. Since MMA and linker beads are repulsive while DEAH beads are attractive to water, it is speculated that the pore spaces between the buckled aggregations are the passages for water diffusing across the shell.

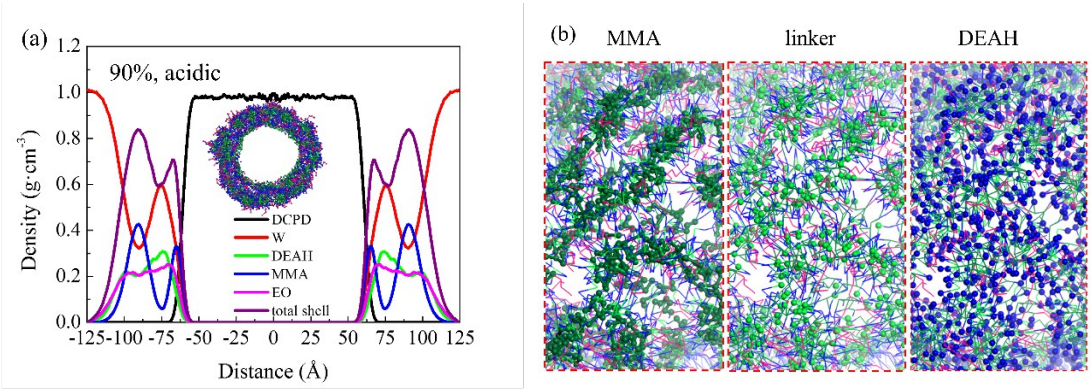

Figure 10. (a) Density profiles of water, polymers and DCPD beads versus the distance from the

center of mass of the microcapsule (crosslinking degree = 90%, ϕ_P : ϕ_D = 12.5% : 7.5%) at low pH. Inset: cross section of the shell. (b) Detailed bead distribution in the 90% crosslinked shell MMA, linker, and DEAH beads are shown as spheres, while the other beads and bonds are as lines.

From high to low pH, the thickness of the crosslinked shell increases from 27.01 Å to 42.18 Å (56%), according to the inner and outer shell radii, r_{in} and r_{out} (half maximum positions of density peaks at the two edges), of total shell density profiles in Figure 7b and 10a. The membrane porosity (t_p) in acidic solution is calculated to be 0.94 based on the formula: $t_p = (V_{acidic} - V_{basic}) / V_{basic}$, where V_{basic} and V_{acidic} are shell volumes in basic and acidic solutions, respectively, and equals to $4\pi(r_{out}^3 - r_{in}^3) / 3$.[24] Combined with the scattered hydrophilic DEAH beads, water diffusivity in the protonated shell is much larger than in the non-protonated shell. The significant change of the shell diffusivity enables an exchange of molecules between solvent and core (for systems in which core molecules are not too hydrophobic)[24,32,58]. The permeability of the crosslinked shell depends on three factors: (1) internal self-repulsion pressure from protonated blocks contributing to shell swelling, (2) crosslinking structures including crosslink degree, length of crosslinking block and length of linker[20,59,60] covalently bonding different blocks and adopt resistance on shell swelling, and (3) compatibility between water (or other solutes) and protonated blocks determining the diffusive drag force of these particles. The “disperse-to-buckle” response of the shell makes the whole structure instable due to uneven distribution of buckled hydrophobic aggregates. We suppose this instability plays an important role

in mitigating the fluid process within the crosslinked shell. Modifications involving the above mentioned factors can be used to regulate the dynamic stability of the protonated shell.

To quantitatively examine the permeability of the crosslinked shell, the *CP* values of shell-shell and shell-W (EO-W, MMA-W and DEA/DEAH-W) in both basic and acidic solutions were plotted as a function of crosslink degree (Figure 11). In basic solution, *CP* is independent of crosslinking, and both the overall shell and the individual polymer beads exhibit contacts in agreement with their relative distributions in the well-packed microcapsule (Figure 7b). For example, $CP_{shell\text{-}shell}$ and $CP_{shell\text{-}W}$ equal to 0.82 and 0.13, respectively, indicating that the shell is closely packed with minimal contact area with water at the shell/water interface, and the permeability of the shell is very low. In acidic solution, $CP_{shell\text{-}shell}$ gradually increases with increasing crosslinking while $CP_{shell\text{-}W}$ (as well as $CP_{EO\text{-}W}$, $CP_{MMA\text{-}W}$ and $CP_{DEAH\text{-}W}$) decrease, corresponding to decreasing porosity (see Figure 8 for morphological evolution). For the 90% model, the $CP_{shell\text{-}shell}$ at low pH is 25% lower compared to high pH, indicating increasing shell porosity. $CP_{MMA\text{-}W}$ and $CP_{DEAH\text{-}W}$ in acidic solution increase by 175% and 2000%, respectively, compared to basic condition, indicating that the affinity between the PDEAEMA block and water has significantly increased (i.e., increased permeability).

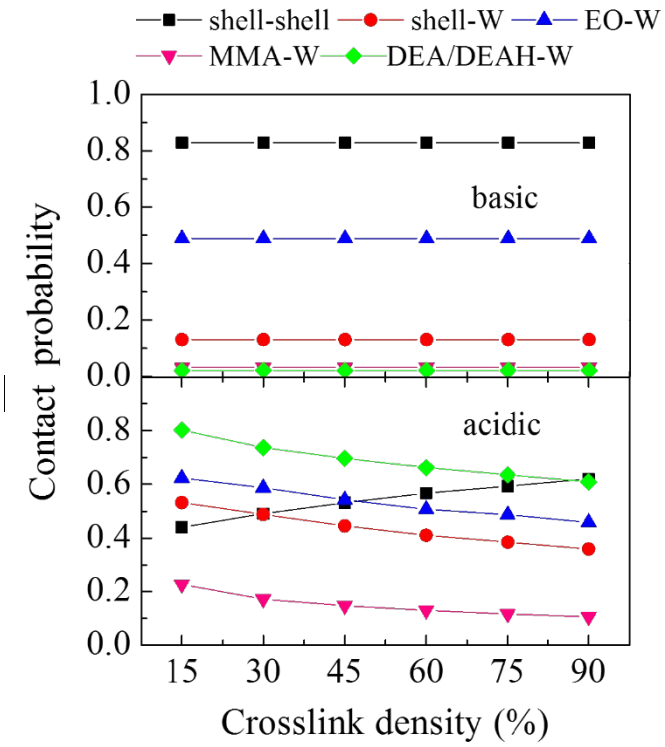

Figure 11. Contact probabilities (*CP*) between water and polymer beads as a function of crosslinking in basic and acidic solutions.

We carried out continuous switching simulations between basic and acidic conditions with a time period of 11.54 ns (i.e., 5.77 ns for each condition). Figure 12 shows the multipulse responses of the contact probabilities of the 90% crosslinked model over four cycles. After an extended de-swollen period (basic condition), the contact probabilities essentially instantaneously switch to the new swollen state (acidic condition). The abrupt variation leads to a period of no change, after which those values are restored with the beginning of the next de-swelling. In our simulations, the time interval is changeable since the contact probabilities show excellent stabilities in both pH environments. The crosslinked shell undergoes a periodic "disperse-to-buckle" transition during cyclical de-swelling and swelling

(Figure S3, Supporting Information). Dynamically, the crosslinked shell is loosened and unsteadily buckled by the backbone MMA beads during swelling. However, elastic forces from the crosslinking nodes restore the distribution of different beads and the dimension of the microcapsule[24,30]. The rapid pH-response and restoration feature of the highly crosslinked block copolymer shell has made it especially attractive for applications where renewable environmental sensitive nanoparticles are needed[24,30].

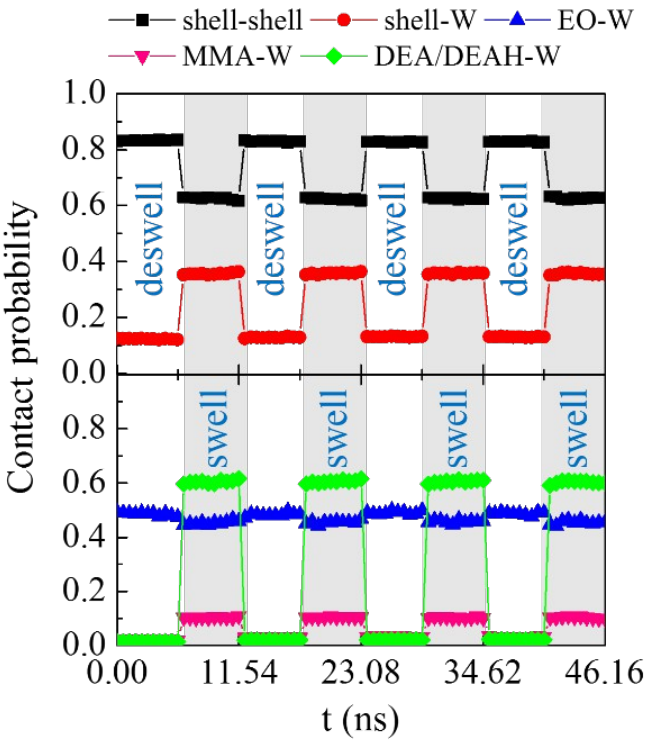

Figure 12. Contact probabilities variations of the 90% crosslinked shell during periodic deswelling (basic, white background) and swelling (acidic, gray background) processes.

3.3. Effect of Block Interaction on Swelling of Microcapsules

To induce a controlled swelling (porosity), the pH-sensitivity of blocks, i.e., self-repulsion variation of the crosslinked shell in response to pH change, plays a profound

effect. This depends on electrostatic and non-electrostatic repulsions between protonated beads and other beads in the model[61]. We systematically studied the tunable porosity of the 90% crosslinked model by simulations with various repulsions between DEAH-MMA, DEAH-DEAH and DEAH-DCPD pairs, which undergo large changes in the repulsive parameter upon pH reduction (Table 1). Figure 13a shows the *CP* values of these bead pairs as a function of $a_{DEAH\text{-}MMA}$, $a_{DEAH\text{-}DEAH}$ and $a_{DEAH\text{-}DCPD}$, respectively. When $a_{DEAH\text{-}MMA}$ is decreased from 146.06 to 25, the attraction between DEAH and MMA is increased, leading to the increase of $CP_{shell\text{-}shell}$ from 0.65 to 0.79 and decrease of $CP_{shell\text{-}W}$ from 0.35 to 0.20 (as well as decrease of $CP_{MMA\text{-}W}$ from 0.10 to 0.03, and $CP_{DEAH\text{-}W}$ from 0.60 to 0.16). When $a_{DEAH\text{-}DEAH}$ is decreased from 150 to 25, the attractive force between DEAH beads is increased, leading to the increase of $CP_{shell\text{-}shell}$ from 0.54 to 0.77 and decrease of $CP_{shell\text{-}W}$ from 0.45 to 0.20 (as well as decrease of $CP_{MMA\text{-}W}$ from 0.16 to 0.03, and $CP_{DEAH\text{-}W}$ from 0.74 to 0.27). Repulsions between DEAH and DCPD beads show no effect on *CP*. Therefore, the structural variation of the crosslinked shell during pH changes is mainly attributed to the interactions of DEAH with itself and with MMA. The crosslinked microcapsule has a widely tunable range of shell swelling (from $CP_{shell\text{-}shell}$ variation) and water permeability (from $CP_{shell\text{-}W}$ variation) in response to environment pH change.

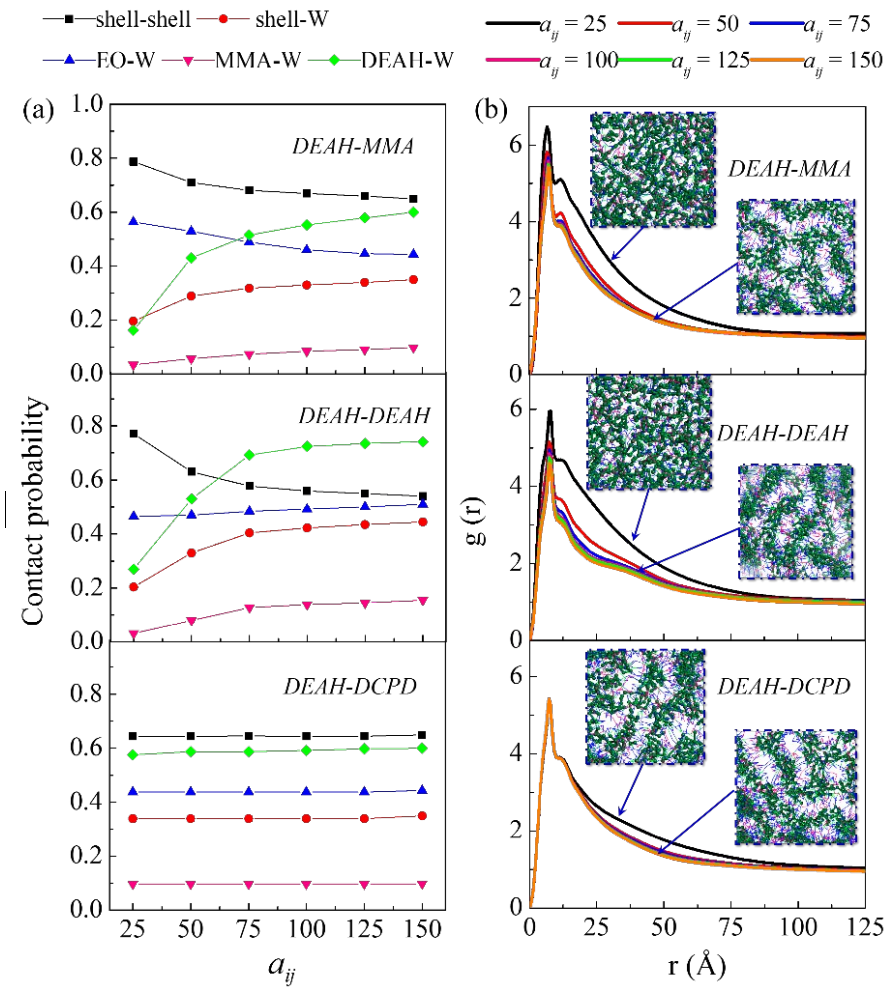

Figure 13. Contact probabilities of shell-shell and shell-water pairs (a), and overall radial distribution functions of the shell (b), at different repulsive parameters between DEAH-MMA, DEAH-DEAH and DEAH-DCPD pairs in acidic solution.

Radial distribution functions of polymers at various repulsions of DEAH-MMA, DEAH-DEAH and DEAH-DCPD pairs were calculated to examine the overall packing of the shell (Figure 13b). The increase of $a_{DEAH\text{-}MMA}$ and $a_{DEAH\text{-}DEAH}$ induce a large decrease of the radial distribution function, corresponding to reduced pairwise probabilities of these beads (i.e., swelling). The insets illustrate the local morphological transitions of the shell from a well-dispersed structure to buckled

structure with increasing DEAH-MMA or DEAH-DEAH repulsions. In addition, the increase of $a_{DEAH\text{-}DCPD}$ leads to a decrease in the range of 25 Å ~ 75 Å. We attribute this regional change to the water molecules near the shell/core interface (Figure 10a). The unaffected short-range (< 25 Å) indicates no shell shrinkage or expansion to the change of DEAH-DCPD repulsion. Again, results show that only repulsions between DEAH-MMA and DEAH-DEAH pairs contribute to the structural variation of the shell.

Our simulations indicate that for a crosslinked block copolymer microcapsule, the swelling rate of the shell depends on the rigidity of the network structure and the sensitivity of functional groups. Through external stimuli the crosslinking mechanically stabilizes the structure, while the functional groups provide driving forces for opening and closing of the shell[15-18,30-32]. To induce controlled swelling, a pH difference which protonates/deprotonates essentially all pH-sensitive groups is also needed[33]. The obtained crosslinked shell can be efficient for both basal and pulsatile penetrations of solutes inward or outward the microcapsule. Once triggered, the transition of the shell configuration is very fast. Overall, the crosslinked block copolymer microcapsules offer a uniquely adaptive and tunable means of carriers that provides effective mechanisms for loading/releasing of drugs or other solutes. For further expansion of the present study, microcapsules with additional crosslinking structures and functional groups can be prepared by modifying the chemistries of linker molecules, stimuli-responsive polymer materials or other additives[1].

4. CONCLUSIONS

We introduced a coarse-grained microcapsule model with a crosslinked shell of pH-sensitive diblock copolymers, PEO-b-PDEAEMA, with tunable particle permeability in response to pH change. DPD was used to reveal the formation and pH-responsive collapse of microcapsules from self-assembly of PEO-b-PDEAEMA/DCPD mixture. Preferential loading of DCPD in PEO-b-PDEAEMA polymers was observed and the mechanism of concentration related encapsulation efficiency of loaded DCPD was uncovered. On reduction of pH, non-covalently bonded shells decompose into small worm-like clusters due to the increased self-repulsion of protonated copolymers. We also see that crosslinking nodes between blocks increase the stability of copolymers and lead to morphologically and kinetically stable polymer shell in acidic solution. A combined effect of crosslinking structure and self-repulsion of the shell was explored and contributed to the large water permeability of the microcapsule on decrease of pH. A “disperse-to-buckle” mechanism was introduced to explain the configurational response of the pH-sensitive crosslinked shell. In particular, the crosslinked shell was efficient in multipulse applications with frequent pH-responses. Finally, the effect of block self-repulsion on the swelling of the crosslinked microcapsule was investigated. To induce a specific swelling rate or extent of the crosslinked shell, both electrostatic and non-electrostatic interactions between protonated beads and others should be controlled. Further studies should be conducted focusing on the modifications of crosslinking structure, stimuli-responsive polymer materials or additives.

ASSOCIATED CONTENT

Supporting Information

The Supporting Information is available free of charge on the ACS Publications website at DOI: XXXXXXXXX.

Self-assembly of pure PEO-b-PDEAEMA polymers; Time variations of the size of the crosslinked shell on pH reduction; Morphological evolution during periodic simulations (PDF)

AUTHOR INFORMATION

Corresponding Author

*E-mail: songqinghu@upc.edu.cn

*E-mail: rfaller@ucdavis.edu

Notes

The authors declare no competing financial interest.

ACKNOWLEDGMENTS

This research was financially supported by the Fundamental Research Funds for the Central Universities (14CX02221A, 16CX06023A and 16CX05017A), the Applied Fundamental Research Foundation of Qingdao Independent Innovation Plan (15-9-1-46-jch and 16-5-1-90-jch), as well as the U.S. Defense Threat Reduction Agency (HDTRA1-15-1-0054). The authors also acknowledge support from the China Scholarship Council.

REFERENCES

(1) Stuart, M. A. C.; Huck, W. T.; Genzer, J.; Müller, M.; Ober, C.; Stamm, M.; Sukhorukov, G. B.; Szleifer, I.; Tsukruk, V. V.; Urban, M. Emerging applications of stimuli-responsive polymer materials. *Nat. Mater.* **2010**, 9, 101-113.

(2) Liu, F.; Urban, M. W. Recent advances and challenges in designing stimuli-responsive polymers. *Prog. Polym. Sci.* **2010**, 35, 3-23.

(3) Marguet, M.; Bonduelle, C.; Lecommandoux, S. Multicompartmentalized polymeric systems: towards biomimetic cellular structure and function. *Chem. Soc. Rev.* **2013**, 42, 512-529.

(4) Huang, X.; Voit, B. Progress on multi-compartment polymeric capsules. *Polym. Chem.* **2013**, 4, 435-443.

(5) De Cock, L. J.; De Koker, S.; De Geest, B. G.; Grooten, J.; Vervaet, C.; Remon, J. P.; Sukhorukov, G. B.; Antipina, M. N. Polymeric multilayer capsules in drug delivery. *Angew. Chem. Int. Ed.* **2010**, 49, 6954-6973.

(6) Du, J.; Tang, Y.; Lewis, A. L.; Armes, S. P. pH-sensitive vesicles based on a biocompatible zwitterionic diblock copolymer. *J. Am. Chem. Soc.* **2005**, 127, 17982-17983.

(7) Qiao, R.; Zhang, X. L.; Qiu, R.; Li, Y.; Kang, Y. S. Fabrication of superparamagnetic cobalt nanoparticles-embedded block copolymer microcapsules. *J. Phys. Chem. C* **2007**, 111, 2426-2429.

(8) Blaiszik, B.; Kramer, S.; Olugebefola, S.; Moore, J. S.; Sottos, N. R.; White, S. R. Self-healing polymers and composites. *Annu. Rev. Mater. Res.* **2010**, 40, 179-211.

(9) Gaitzsch, J.; Huang, X.; Voit, B. Engineering functional polymer capsules toward smart nanoreactors. *Chem. Rev.* **2015**, 116, 1053-1093.

(10) Piogé, S.; Nesterenko, A.; Brotons, G.; Pascual, S.; Fontaine, L.; Gaillard, C.;

Nicol, E. Core cross-linking of dynamic diblock copolymer micelles: Quantitative study of photopolymerization efficiency and micelle structure. *Macromolecules* **2011**, 44, 594-603.

(11) Laskar, P.; Dey, J.; Ghosh, S. k. Evaluation of zwitterionic polymersomes spontaneously formed by pH-sensitive and biocompatible PEG based random copolymers as drug delivery systems. *Colloid Surface B* **2016**, 139, 107-116.

(12) Mai, Y.; Eisenberg, A. Self-assembly of block copolymers. *Chem. Soc. Rev.* **2012**, 41, 5969-5985.

(13) Moughton, A. O.; Hillmyer, M. A.; Lodge, T. P. Multicompartment block polymer micelles. *Macromolecules* **2011**, 45, 2-19.

(14) Rabnawaz, M.; Liu, G. Preparation and application of a dual light-responsive triblock terpolymer. *Macromolecules* **2012**, 45, 5586-5595.

(15) Shi, Y.; van Nostrum, C. F.; Hennink, W. E. Interfacially Hydrazone cross-linked thermosensitive polymeric micelles for acid-triggered release of paclitaxel. *ACS Biomater. Sci. Eng.* **2015**, 1, 393-404.

(16) Sun, G.; Cui, H.; Lin, L. Y.; Lee, N. S.; Yang, C.; Neumann, W. L.; Freskos, J. N.; Shieh, J. J.; Dorshow, R. B.; Wooley, K. L. Multicompartment polymer nanostructures with ratiometric dual-emission pH-sensitivity. *J. Am. Chem. Soc.* **2011**, 133, 8534.

(17) Lee, N. S.; Sun, G.; Neumann, W. L.; Freskos, J. N.; Shieh, J. J.; Dorshow, R. B.; Wooley, K. L. Photonic shell-crosslinked nanoparticle probes for optical imaging and monitoring. *Adv. Mater.* **2009**, 21, 1344-1348.

(18) Kadam, V. S.; Nicol, E.; Gaillard, C. Synthesis of flower-like poly (ethylene oxide) based macromolecular architectures by photo-cross-linking of block copolymers self-assemblies. *Macromolecules* **2011**, 45, 410-419.

(19) Sun, G.; Lee, N. S.; Neumann, W. L.; Freskos, J. N.; Shieh, J. J.; Dorshow, R. B.; Wooley, K. L. A fundamental investigation of cross-linking efficiencies within discrete nanostructures, using the cross-linker as a reporting molecule. *Soft Matter* **2009**, 5, 3422-3429.

(20) Huang, X.; Appelhans, D.; Formanek, P.; Simon, F.; Voit, B. Tailored synthesis of intelligent polymer nanocapsules: an investigation of controlled permeability and pH-dependent degradability. *ACS Nano* **2012**, 6, 9718-9726.

(21) Kim, K. T.; Zhu, J.; Meeuwissen, S. A.; Cornelissen, J. J.; Pochan, D. J.; Nolte, R. J.; van Hest, J. C. Polymersome stomatocytes: controlled shape transformation in polymer vesicles. *J. Am. Chem. Soc.* **2010**, 132, 12522-12524.

(22) Kim, M. S.; Lee, D. S. Biodegradable and pH-sensitive polymersome with tuning permeable membrane for drug delivery carrier. *Chem. Commun.* **2010**, 46, 4481-4483.

(23) Carlsen, A.; Glaser, N.; Le Meins, J.-F. o.; Lecommandoux, S. b. Block copolymer vesicle permeability measured by osmotic swelling and shrinking. *Langmuir* **2011**, 27, 4884-4890.

(24) Masoud, H.; Alexeev, A. Controlled release of nanoparticles and macromolecules from responsive microgel capsules. *ACS Nano* **2011**, 6, 212-219.

(25) Hong, W.; Zhao, X.; Zhou, J.; Suo, Z. A theory of coupled diffusion and large

deformation in polymeric gels. *J. Mech. Phys. Solids* **2008**, 56, 1779-1793.

(26) Durbin, E. W.; Buxton, G. A. A coarse-grained model of targeted drug delivery from responsive polymer nanoparticles. *Soft Matter* **2010**, 6, 762-767.

(27) Ding, H.-m.; Ma, Y.-q. Controlling cellular uptake of nanoparticles with pH-sensitive polymers. *Sci. Rep.* **2013**, 3, 2804.

(28) Sun, M.; Li, B.; Li, Y.; Liu, Y.; Liu, Q.; Jiang, H.; He, Z.; Zhao, Y.; Sun, J. Experimental observations and dissipative particle dynamic simulations on microstructures of pH-sensitive polymer containing amorphous solid dispersions. *Int. J. Pharmaceut.* **2017**, 517, 185-195.

(29) Wang, Y.; Ren, J. W.; Zhang, C. Y.; He, M. C.; Wu, Z. M.; Guo, X. D. Compatibility studies between an amphiphilic pH-sensitive polymer and hydrophobic drug using multiscale simulations. *RSC Adv.* **2016**, 6, 101323-101333.

(30) Luo, Z.; Li, Y.; Wang, B.; Jiang, J. pH-sensitive vesicles formed by amphiphilic grafted copolymers with tunable membrane permeability for drug loading/release: A multiscale simulation study. *Macromolecules* **2016**, 49, 6084-6094.

(31) Luo, Z.; Jiang, J. pH-sensitive drug loading/releasing in amphiphilic copolymer PAE–PEG: Integrating molecular dynamics and dissipative particle dynamics simulations. *J. Controlled Release* **2012**, 162, 185-193.

(32) Nie, S. Y.; Lin, W. J.; Yao, N.; Guo, X. D.; Zhang, L. J. Drug release from ph-sensitive polymeric micelles with different drug distributions: insight from

coarse-grained simulations. *ACS Appl. Mater. Inter.* **2014**, 6, 17668-17678.

(33) Nie, S. Y.; Sun, Y.; Lin, W. J.; Wu, W. S.; Guo, X. D.; Qian, Y.; Zhang, L. J. Dissipative particle dynamics studies of doxorubicin-loaded micelles assembled from four-arm star triblock polymers 4AS-PCL-b-PDEAEMA-b-PPEGMA and their pH-release mechanism. *J. Phys. Chem. B* **2013**, 117, 13688-13697.

(34) Shenogina, N. B.; Tsige, M.; Patnaik, S. S.; Mukhopadhyay, S. M. Molecular modeling approach to prediction of thermo-mechanical behavior of thermoset polymer networks. *Macromolecules* **2012**, 45, 5307-5315.

(35) Wu, C.; Xu, W. Atomistic molecular modelling of crosslinked epoxy resin. *Polymer* **2006**, 47, 6004-6009.

(36) Wang, Z.; Lv, Q.; Chen, S.; Li, C.; Sun, S.; Hu, S. Glass transition investigations on highly crosslinked epoxy resins by molecular dynamics simulations. *Mol. Simulat.* **2015**, 41, 1515-1527.

(37) Wu, C.; Xu, W. Atomistic molecular simulations of structure and dynamics of crosslinked epoxy resin. *Polymer* **2007**, 48, 5802-5812.

(38) Wang, Z.; Lv, Q.; Chen, S.; Li, C.; Sun, S.; Hu, S. Effect of interfacial bonding on interphase properties in SiO_2/epoxy nanocomposite: A molecular synamics simulation study. *ACS Appl. Mater. Inter.* **2016**, 8, 7499-7508.

(39) Masoud, H.; Alexeev, A. Permeability and diffusion through mechanically deformed random polymer networks. *Macromolecules* **2010**, 43, 10117-10122.

(40) Quesada-Pérez, M.; Ramos, J.; Forcada, J.; Martín-Molina, A. Computer simulations of thermo-sensitive microgels: Quantitative comparison with

experimental swelling data. *J. Chem. Phys.* **2012**, 136, 244903.

(41) Rumyantsev, A. M.; Rudov, A. A.; Potemkin, I. I. Intraparticle segregation of structurally homogeneous polyelectrolyte microgels caused by long-range Coulomb repulsion. *J. Chem. Phys.* **2015**, 142, 171105..

(42) Tan, J.; Too, H.; Hatton, T.; Tam, K. Aggregation behavior and thermodynamics of binding between poly (ethylene oxide)-block-poly (2-(diethylamino) ethyl methacrylate) and plasmid DNA. *Langmuir* **2006**, 22, 3744-3750.

(43) Tan, J.; Ravi, P.; Too, H.-P.; Hatton, T. A.; Tam, K. Association behavior of biotinylated and non-biotinylated poly (ethylene oxide)-b-poly (2-(diethylamino) ethyl methacrylate). *Biomacromolecules* **2005**, 6, 498-506.

(44) Xu, F. J.; Yang, W. T. Polymer vectors via controlled/living radical polymerization for gene delivery. *Prog. Polym. Sci.* **2011**, 36, 1099-1131.

(45) Tan, J.; Hatton, T.; Tam, K.; Too, H. Correlating transfection barriers and biophysical properties of cationic polymethacrylates. *Biomacromolecules* **2007**, 8, 448-454.

(46) Yuan, W.; Zhang, J.; Wei, J.; Zhang, C.; Ren, J. Synthesis and self-assembly of pH-responsive amphiphilic dendritic star-block terpolymer by the combination of ROP, ATRP and click chemistry. *Eur. Polym. J.* **2011**, 47, 949-958.

(47) Hoogerbrugge, P.; Koelman, J. Simulating microscopic hydrodynamic phenomena with dissipative particle dynamics. *EPL-Europhys. Lett.* **1992**, 19, 155.

(48) Groot, R. D.; Warren, P. B. Dissipative particle dynamics: Bridging the gap

between atomistic and mesoscopic simulation. *J. Chem. Phys.* **1997**, 107, 4423-4435.

(49) Wang, W.; Anderson, N. A.; Travesset, A.; Vaknin, D. Regulation of the electric charge in phosphatidic acid domains. *J. Phys. Chem. B* **2012**, 116, 7213-7220.

(50) Shuichi, N. Constant temperature molecular dynamics methods. *Prog. Theor. Phys. Supp.* **1991**, 103, 1-46.

(51) Berendsen, H. J.; Postma, J. v.; van Gunsteren, W. F.; DiNola, A.; Haak, J. Molecular dynamics with coupling to an external bath. *J. Chem. Phys.* **1984**, 81, 3684-3690.

(52) Isele-Holder, R. E.; Rabideau, B. D.; Ismail, A. E. Definition and computation of intermolecular contact in liquids using additively weighted voronoi tessellation. *J. Phys. Chem. A* **2012**, 116, 4657-4666.

(53) Rycroft, C. Voro++: A three-dimensional Voronoi cell library in C++. *Lawrence Berkeley National Laboratory* **2009**.

(54) Mable, C. J.; Gibson, R. R.; Prevost, S.; McKenzie, B. E.; Mykhaylyk, O. O.; Armes, S. P. Loading of silica nanoparticles in block copolymer vesicles during polymerization-induced self-assembly: encapsulation efficiency and thermally triggered release. *J. Am. Chem. Soc.* **2015**, 137, 16098.

(55) Tam, Y. T.; Gao, J.; Kwon, G. S. Oligo (lactic acid) n-paclitaxel prodrugs for poly (ethylene glycol)-block-poly (lactic acid) micelles: loading, release, and backbiting conversion for anticancer activity. *J. Am. Chem. Soc.* **2016**, 138, 8674-8677.

(56) Du, J.; Armes, S. P. pH-responsive vesicles based on a hydrolytically self-cross-linkable copolymer. *J. Am. Chem. Soc.* **2005**, 127, 12800-12801.

(57) Yu, S.; Azzam, T.; Rouiller, I.; Eisenberg, A. “Breathing” vesicles. *J. Am. Chem. Soc.* **2009**, 131, 10557-10566.

(58) Chen, H.; Ruckenstein, E. Formation and degradation of multicomponent multicore micelles: insights from dissipative particle dynamics simulations. *Langmuir* **2013**, 29, 5428-5434.

(59) Kamerlin, N.; Elvingson, C. Collapse dynamics of core-shell nanogels. *Macromolecules* **2016**, 49, 5740-5749.

(60) Varga, I.; Gilányi, T.; Meszaros, R.; Filipcsei, G.; Zrinyi, M. Effect of cross-link density on the internal structure of poly (N-isopropylacrylamide) microgels. *J. Phys. Chem. B* **2001**, 105, 9071-9076.

(61) Yi, Q.; Wen, D.; Sukhorukov, G. B. UV-cross-linkable multilayer microcapsules made of weak polyelectrolytes. *Langmuir* **2012**, 28, 10822-10829.

For Table of Contents use only:

Tunable Permeability of Crosslinked Microcapsules from pH-Responsive Amphiphilic Diblock Copolymers: A Dissipative Particle Dynamics Study

Zhikun Wang[1,2], Jianbang Gao[1], Vincent Ustach[2], Chunling Li[1,3], Shuangqing Sun[1,3], Songqing Hu[1,3,*], Roland Faller[2,*]

[1]*College of Science, China University of Petroleum (East China), 266580 Qingdao, Shandong, China*

[2]*Department of Chemical Engineering, UC Davis, 95616 Davis, California, USA*

[3]*Key Laboratory of New Energy Physics & Materials Science in Universities of Shandong, China University of Petroleum (East China), 266580 Qingdao, Shandong, China*